

# Two-dimensional solitons in dipolar Bose-Einstein condensates with spin-orbit coupling

Xunda Jiang<sup>1</sup>, Zhiwei Fan<sup>1</sup>, Zhaopin Chen<sup>1,2</sup>, Wei Pang<sup>3</sup>, Yongyao Li<sup>1,\*</sup> and Boris A. Malomed<sup>2</sup>

<sup>1</sup>*Department of Applied Physics, College of Electronic Engineering,  
South China Agricultural University, Guangzhou 510642, China*

<sup>2</sup>*Department of Physical Electronics, School of Electrical Engineering,  
Faculty of Engineering, Tel Aviv University, Tel Aviv 69978, Israel.*

<sup>3</sup>*Department of Experiment Teaching, Guangdong University of Technology, Guangzhou 510006, China*

We report families of two-dimensional (2D) composite solitons in spinor dipolar Bose-Einstein condensates, with two localized components linearly mixed by the spin-orbit coupling (SOC), and the intrinsic nonlinearity represented by the dipole-dipole interaction (DDI) between atomic magnetic moments polarized in-plane by an external magnetic field. Recently, stable solitons were predicted in the form of *semi-vortices* (composites built of coupled fundamental and vortical components) in the 2D system combining the SOC and contact attractive interactions. Replacing the latter by the anisotropic long-range DDI, we demonstrate that, for a fixed norm of the soliton, the system supports a *continuous family* of stable spatially asymmetric vortex solitons (AVSs), parameterized by an offset of the pivot of the vortical component relative to its fundamental counterpart. The offset is limited by a certain maximum value, while the energy of the AVS practically does not depend on the offset. At small values of the norm, the vortex solitons are subject to a weak oscillatory instability. In the present system, with the Galilean invariance broken by the SOC, the composite solitons are set in motion by a kick whose strength exceeds a certain depinning value. The kicked solitons feature a negative effective mass, drifting along a spiral trajectory opposite to the direction of the kick. A critical angular velocity, up to which the semi-vortices may follow rotation of the polarizing magnetic field, is found too.

PACS numbers: 03.75.Lm; 05.45.Yv; 03.75.Mn

## I. INTRODUCTION

The creation of stable two- and three-dimensional (2D and 3D) self-trapped modes (bright solitons and solitary vortices) in various physical media, including optical waveguides and atomic Bose-Einstein condensates (BECs), had been identified as a challenging problem some time ago [1, 2], retaining this status up to now. A fundamental difficulty is that, while the ubiquitous cubic self-focusing nonlinearity, which represents the Kerr effect in optics [3] and attractive inter-atomic collisions in BEC [the latter may be controlled by means of the Feshbach resonance (FR) [4–6]], readily creates stable solitons in the 1D geometry, all localized multidimensional modes supported by the cubic self-focusing are unstable. They are destroyed by the critical [7–9] or supercritical [8, 9] collapse, which is driven by the cubic attractive nonlinearity in the 2D and 3D, respectively. 2D and 3D bright solitons with embedded vorticity are subject to a still stronger instability against splitting by perturbations breaking their axial symmetry [1, 2].

A possibility for the stabilization of multidimensional solitons is suggested by using self-focusing nonlinearity weaker than cubic. Indeed, quadratic (alias second-harmonic-generating) nonlinearity does not cause collapse in 2D and 3D geometries, hence it may be used for making stable fundamental solitons, as demonstrated experimentally in the 2D spatial domain [10], and shown, both theoretically [11] and experimentally [12], for 2D spatiotemporal “optical bullets” [12]. However, the quadratic nonlinearity does not remove the azimuthal splitting instability of vortex solitons [13, 14].

Both fundamental and vortex bright solitons may be made stable using combinations of competing self-focusing and self-defocusing nonlinear terms, namely, cubic-quintic [15–18] or quadratic-cubic [19]. In these settings, all the fundamental solitons are stable (indeed, the creation of 2D stable spatial solitons in a colloidal optical waveguide, featuring the cubic-quintic nonlinearity, has been recently reported [20]), while vortex solitons are stabilized above a specific threshold, which actually implies that they must be very broad, making their experimental creation difficult.

The most straightforward means for the stabilization of fundamental and vortical solitons in 2D and 3D geometries is provided by the use of spatially periodic potentials. In optical media, such potentials can be imposed in the form

---

\*Electronic address: yongyaoli@gmail.com

of virtual photonic lattices in photorefractive crystals [21], and permanent lattices written in bulk silica [22], while in BEC similar potentials are induced by interference patterns (optical lattices) created by laser beams illuminating the condensate [23]. In the experiment, photonic-lattice potentials were used to make stable 2D fundamental and vortex optical solitons [24–27], as well as 3D spatiotemporal “bullets” [28]. A recent experimental result is the creation of 2D plasmon-polariton solitons in microcavities, which are also supported by a lattice structure [29].

Another possibility for the stabilization of 2D fundamental solitons is offered by “management” techniques, i.e., periodic alternation of the sign of the nonlinearity [30]. This possibility was originally proposed for the transmission of optical beams across a medium built as a periodic alternation of layers of self-focusing and defocusing materials [31]. The relevance of the same method for the stabilization of 2D matter-wave solitons in BEC was demonstrated too, with the help of periodic switch of the sign of the cubic nonlinearity by means of the FR [32–34]. However, the management cannot stabilize 2D solitary vortices, nor 3D fundamental solitons.

A completely different approach to the creation of self-trapped fundamental and vortex modes was recently proposed in Ref. [35–39]. It relies on the use of *self-defocusing* nonlinearity, whose local strength in the space of dimension  $D$  grows from the center to periphery, as a function of distance  $r$ , at any rate faster than  $r^D$ , supporting extremely robust families of solitons, solitary vortices, and more complex modes, such as *hopfions*, which carry two different topological charges [40], for  $D = 1, 2, 3$ .

A new possibility was recently revealed by the theoretical analysis of two-component (spinor) BEC with the linear spin-orbit coupling (SOC) between the components, that may be induced by a combination of appropriate optical and magnetic fields [41]–[44]. In most cases, the SOC is considered in the combination with the repulsive collisional nonlinearity, which may give rise to delocalized (“dark”) vortices in the 2D setting [45–49] and gap solitons of the bright type, if a lattice potential is included [50–52]. It is also possible to consider the interplay of the SOC with the intrinsic attractive nonlinearity. The latter setting easily supports 1D solitons [53–55]. An unexpected result was recently produced by the consideration of the 2D self-attractive SOC system: while it was previously believed that any system with the cubic self-focusing would give rise to unstable solitons in the free 2D space, in view of the simultaneous occurrence of the *critical collapse* [7–9], the SOC system (in particular, of the Rashba type) creates *stable* solitons of *semi-vortex* and *mixed-mode* types, with one fundamental ( $\psi_+$ ) and one vortex ( $\psi_-$ ) wave-function components, or a mixture of fundamental and vortex modes in both components, respectively [56–58]. Although the SOC terms in the respective Gross-Pitaevskii equations (GPEs) break the rotational invariance [see Eq. (3) below], the two components of the semi-vortex solution, with chemical potential  $\mu$ , feature the axial symmetry in polar coordinates  $(r, \theta)$ ,

$$\psi_+(r, \theta, t) = e^{-i\mu t} f_1(r^2), \quad \psi_-(r, \theta, t) = e^{-i\mu t + i\theta} r f_2(r^2), \quad (1)$$

while the mixed modes do not maintain this symmetry, and cannot be represented by an exact ansatz similar to Eq. (1) [56]. This ansatz, as well as more complex mixed-mode solutions (they are stable if the attraction between  $\psi_+$  and  $\psi_-$  is stronger than the self-attraction of the components), clearly demonstrate that the SOC makes two components of the soliton’s spinor wave function topologically different. Mobile 2D mixed-mode solitons were found too, which is a nontrivial issue, as the SOC breaks the Galilean invariance of the system [56]. Furthermore, the same stabilization mechanism was elaborated for 2D spatiotemporal solitons in a dual-core planar optical waveguide, with SOC emulated by dispersive linear coupling between the two cores [59]. An explanation to these findings is provided by the fact that the dimensionality of the SOC coefficient defines a spatial scale in the system; thus, it breaks the scaling invariance of the underlying 2D GPEs with the cubic terms, and lifts the related degeneracy of the norm of the two-component solitons, placing them *below* the threshold for the onset of the collapse. Being thus protected against the collapse, the self-trapped 2D solitons become stable objects, which realize the ground state of the 2D setting.

It is easier to predict stable multidimensional solitons in media with nonlocal cubic nonlinearities, where the collapse does not occur. In optics, the nonlocality is featured by reorientational nonlinearity of liquid crystals [60–62], as well as by thermal response of a dielectric medium [63–65]. In BEC, effective nonlocal nonlinearities originate from the isotropic Van der Waals interactions between Rydberg atoms [66], and long-range dipole-dipole interactions (DDIs) of atoms carrying permanent magnetic dipole moments [67–70]. In the latter context, stable 1D bright and dark solitons [71, 72], 2D bright solitons [73], 3D dark solitons [74], and bright solitary vortices [75] were predicted, assuming that attractive DDI can be (artificially) realized in isotropic configurations. On the other hand, fundamental and vortex solitons, in the 1D and 2D geometry alike, may be readily made stable in the natural setting with repulsive DDIs between field-induced (rather than permanent) atomic moments oriented perpendicular to the system’s plane, if the strength of the polarizing field (magnetic or electric) grows from the center to periphery faster than  $r^3$  [76]. In a more realistic anisotropic 2D setting with the *in-plane* polarization of permanent atomic moments, stable fundamental (zero-vorticity) solitons were predicted too [77, 78]. A challenging problem, which was not explored before, is a possibility of existence of *anisotropic solitary vortices*, i.e., anisotropic bright solitons, supported by the DDI, with an embedded topological charge that may be interpreted as vorticity.

The objective of the present work is to construct stable 2D topological solitons in the model of the spinor BEC with the in-plane polarization of atomic moments, combining the linear SOC (of the Rashba type) and nonlinear long-range

DDI. The SOC-DDI system was introduced, in a form relevant to the experimental implementation, in Refs. [79–81]. 2D fundamental solitons in the system of this type, which includes the attractive DDI and local repulsive nonlinearity, were recently investigated in Ref. [82] (to focus on the most interesting situation, we here consider only the DDI nonlinearity). Modes of two kinds were found in the latter work, *viz.*, smooth solitons with a spatially varying phase, and stripe solitons with a spatially oscillating density, similar to those which were reported in Ref. [57], that was dealing with a combination of the SOC, attractive local nonlinearity, and lattice potentials in 2D. Mobility of the 2D solitons was also addressed in Ref. [82].

In this work, we report stable 2D topological solitons, in the form of spatially symmetric and asymmetric semi-vortices. The asymmetry is represented by separation between the pivot of the vortex component and central point of its fundamental counterpart, which breaks the system's reflectional symmetry,

$$(x, y) \rightarrow (-x, -y), \quad (\psi_+, \psi_-) \rightarrow (\psi_+, -\psi_-). \quad (2)$$

To the best of our knowledge, this is the first example of stable asymmetric vortex solitons (AVSs) found in any nonlinear system. In particular, they are completely different from azimuthons found in isotropic media with local [83–86] or nonlocal [87] interactions. Simultaneously, the AVSs offer the first example of 2D vortical solitons supported by the anisotropic in-plane DDI.

The paper is structured as follows. The model is introduced in Section II. Basic results for stationary symmetric vortex solitons (SVSs) and their mobility are presented in Section III. In Section IV, we consider AVSs, which, as said above, feature a symmetry-breaking shift between the vortex and fundamental components. The possibility of setting SVSs and AVSs into rotation is addressed in Section V. The paper is concluded by section VI.

## II. THE MODEL

In the mean-field approximation, the binary dipolar BEC is governed by the system of coupled GPEs for the spinor wave function,  $\psi = (\psi_+, \psi_-)$ , written here in the scaled 2D form:

$$\begin{aligned} i \frac{\partial \psi_+}{\partial t} &= -\frac{1}{2} \nabla^2 \psi_+ + \lambda \left( \frac{\partial \psi_-}{\partial x} - i \frac{\partial \psi_-}{\partial y} \right) \\ &+ \psi_+(\mathbf{r}) \int \int d\mathbf{r}' R(\mathbf{r} - \mathbf{r}') [|\psi_+(\mathbf{r}')|^2 + |\psi_-(\mathbf{r}')|^2], \\ i \frac{\partial \psi_-}{\partial t} &= -\frac{1}{2} \nabla^2 \psi_- - \lambda \left( \frac{\partial \psi_+}{\partial x} + i \frac{\partial \psi_+}{\partial y} \right) \\ &+ \psi_-(\mathbf{r}) \int \int d\mathbf{r}' R(\mathbf{r} - \mathbf{r}') [|\psi_-(\mathbf{r}')|^2 + |\psi_+(\mathbf{r}')|^2]. \end{aligned} \quad (3)$$

Here  $\lambda$  is the Rashba-SOC coefficient, the contact nonlinearity is neglected, as said above, and the DDI kernel is

$$R(\mathbf{r} - \mathbf{r}') = \frac{1 - 3 \cos^2 \Theta}{[\epsilon^2 + (\mathbf{r} - \mathbf{r}')^2]^{3/2}}, \quad (4)$$

where  $\epsilon$  is a regularization scale, which is determined by the transverse size of the nearly-2D layer [71, 88]. The form of this kernel implies that the dipoles are polarized, by an external magnetic field, in the 2D plane along the positive direction of the  $x$  axis, hence  $\cos^2 \Theta \equiv (x - x')^2 / |\mathbf{r} - \mathbf{r}'|^2$ . Adequate results, with a characteristic size of 2D solitons being much larger than  $\epsilon$  (otherwise, the solitons are not quasi-2D objects), can be produced, e.g., with  $\epsilon = 0.05$ , if  $\lambda = 1$  is set by scaling. These values of  $\epsilon$  and  $\lambda$  are fixed below.

An essential peculiarity of Eqs. (3) and (4) is the interplay of two different kinds of the spatial anisotropy, which are introduced, severally, by the linear SOC and nonlinear DDI terms. While the DDI anisotropy is characterized by the form of kernel (4), the structure of the SOC Hamiltonian of the Rashba type, acting on spinor  $(\psi_+, \psi_-)^T$  in Eq. (3), is elucidated by writing it in the polar coordinates:

$$\mathbf{H}_{\text{SOC}}^{(\text{Ra})} = \lambda (\sigma_x \hat{p}_y - \sigma_y \hat{p}_x) = \lambda \left( \begin{array}{cc} 0 & e^{-i\theta} \left( \frac{\partial}{\partial r} - \frac{i}{r} \frac{\partial}{\partial \theta} \right) \\ -e^{+i\theta} \left( \frac{\partial}{\partial r} + \frac{i}{r} \frac{\partial}{\partial \theta} \right) & 0 \end{array} \right), \quad (5)$$

where  $\mathbf{p} = -i\nabla$  is the momentum operator, and  $\sigma_{x,y}$  are the Pauli matrices. In particular, this structure makes it clear why ansatz (1) produces the exact solution in the model with the contact interactions.

The remaining symmetries of Eq. (3) correspond to the invariance with respect to the specular reflections in the  $x$  and  $y$  directions:

$$x \rightarrow -x, t \rightarrow -t, \psi_{\pm} \rightarrow \pm\psi_{\pm}^*, \quad (6)$$

$$y \rightarrow -y, t \rightarrow -t, \psi_{\pm} \rightarrow \psi_{\pm}^*, \quad (7)$$

where  $*$  stands for the complex conjugate, and, independently, to the invariance with respect to the flip of the two components of the (pseudo-) spinor wave function:

$$\psi_+ \rightleftharpoons \psi_-, x \rightarrow -x. \quad (8)$$

In particular, the above-mentioned inversion transformation, defined as per Eq. (2), is a product of reflections (6) and (7).

Stationary solitons are introduced as usual,

$$\{\psi_+(\mathbf{r}, t), \psi_-(\mathbf{r}, t)\} = \{\phi_+(\mathbf{r}), \phi_-(\mathbf{r})\} e^{-i\mu t}, \quad (9)$$

with total norm

$$N = N_+ + N_- = \int \int |\psi_+(\mathbf{r})|^2 d\mathbf{r} + \int \int |\psi_-(\mathbf{r})|^2 d\mathbf{r}, \quad (10)$$

and energy

$$E = E_{\text{kin}} + E_{\text{SOC}} + E_{\text{DDI}}, \quad (11)$$

$$\begin{aligned} E_{\text{kin}} &= \frac{1}{2} \int \int d\mathbf{r} (|\nabla\phi_+|^2 + |\nabla\phi_-|^2), \\ E_{\text{SOC}} &= \frac{\lambda}{2} \int \int d\mathbf{r} \left[ \phi_+^* \left( \frac{\partial\phi_-}{\partial x} - i \frac{\partial\phi_-}{\partial y} \right) + \phi_-^* \left( -\frac{\partial\phi_+}{\partial x} - i \frac{\partial\phi_+}{\partial y} \right) + \text{c.c} \right], \\ E_{\text{DDI}} &= \frac{1}{2} \int \int d\mathbf{r} d\mathbf{r}' R(\mathbf{r} - \mathbf{r}') [|\phi_+(\mathbf{r})|^2 + |\phi_-(\mathbf{r})|^2] (|\phi_+(\mathbf{r}')|^2 + |\phi_-(\mathbf{r}')|^2). \end{aligned} \quad (12)$$

$N$  and  $E$  are dynamical invariants of the system, along with the linear momentum,  $i \int \int d\mathbf{r} (\phi_+ \nabla\phi_+^* + \phi_- \nabla\phi_-^*)$  [it remains conserved, in spite of the breaking of the Galilean invariance by the SOC terms in Eq. (3)], while the conservation of the angular momentum is broken by both the SOC and DDI terms.

### III. SYMMETRIC VORTEX SOLITONS (SVSS)

#### A. Quiescent solitons

Unlike the SOC model with contact attractive interactions, the anisotropic DDI in Eq. (3) does not admit any exact ansatz for semi-vortices, cf. Eq. (1). A variational approximation for the stationary states can be developed, but it turns out to be very cumbersome. Therefore, stationary SVS solutions were found by means of the imaginary-time-integration method [89, 90], and their stability was tested by means of real-time simulations. All the numerical results were produced using square-shaped numerical grids with mesh sizes  $\delta x = \delta y$ . The input for the imaginary-time simulations was taken as a semi-vortex, using the above-mentioned ansatz (1) as a pattern:

$$\phi_+^{(0)} = A_+ \exp(-\alpha_+ r^2), \quad \phi_-^{(0)} = A_- r e^{i\theta} \exp(-\alpha_- r^2), \quad (13)$$

where  $A_{1,2}$  and  $\alpha_{1,2} > 0$  are real constants. In the course of the evolution in imaginary time, the mode was deformed, but its topological structure persisted.

Numerically generated results demonstrates that the solitons are stable if the total norm exceeds a certain threshold,  $N > N_{\text{th}} \approx 0.12$ . A typical example of the output in the form of *stable* SVSs with norm  $N = 0.15$  is displayed in Fig. 1(a). In this figure, it is clearly seen that both components feature a typical anisotropic structure, being stretched along the horizontal axis, which is easily explained by the fact that DDI kernel (4) implies the attractive interaction along  $x$ , i.e., for  $\Theta = 0$  and, more generally, for  $\cos^2 \Theta < 1/3$  [77, 78]. On the other hand, the density patterns in both components of the semi-vortex are symmetric with respect to the  $x$  and  $y$  axes [i.e., they are invariant with respect

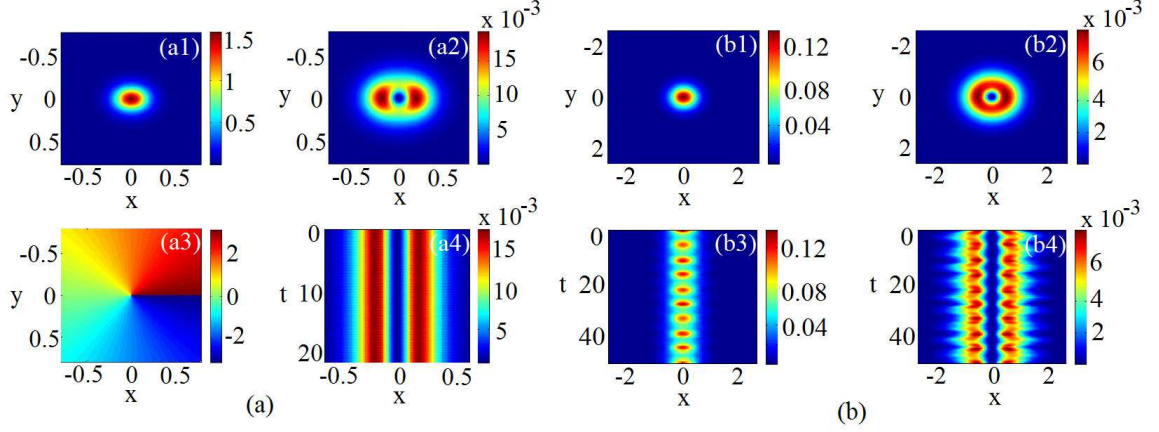


FIG. 1: (Color online) (a) The stable SVS with total norm  $N = 0.15$ . (a1,a2) Intensity distributions of the fundamental and vortical components,  $|\phi_+(x, y)|^2$  and  $|\psi_-(x, y)|^2$ , respectively. (a3) The phase structure of the vortical component. (a4) Direct real-time simulations corroborating the stability of this SVS (the evolution of the vortical component is displayed in cross section  $y = 0$ ). The evolution time in this panel exceeds 100 characteristic diffraction times of the soliton. (b) An unstable SVS with  $N = 0.10$ . (b1,b2) The same as in (a1,a2), for the unstable SVS. (b3,b4) Real-time simulations show the oscillatory instability of both components, in cross section  $y = 0$ , by means of the density contour plots. The resulting breathers keeps the vorticity and symmetries of the original SVS.

to transformations (6) and (7)], that is why this soliton is called SVS. When the norm below  $N_{\text{th}}$ , the semi-vortex develops an oscillatory instability, which converts it into a breather. Nevertheless, the original topological structure and symmetries of the SVS are held by the robust breather, as shown in Fig. 1(b3,b4); in addition to the oscillations displayed in that figure, the elliptically deformed vortex component ( $\psi_-$ ) performs periodic “nutations”, with its axes oscillating around the average directions.

It is relevant to stress that such a stability threshold for the semi-vortex solitons, in terms of the norm, is different from the stability conditions found in the system combining the SOC and contact attractive interactions, where the solitons remain stable from arbitrarily small values of  $N$  up to the collapse threshold [56]. In that system, the stability is determined by the fact that the spatial scale, introduced by the SOC, breaks the scaling invariance of the 2D GPE, pushing the soliton’s norm below the collapse-onset threshold, thus securing the stability against the collapse [56]. For the system with the nonlocal interaction considered here, the stability is, in a sense, easier to achieve, as the long-range DDI by itself does not lead to the collapse.

To quantify properties of the entire SVS family, we define the following characteristics of these self-trapped modes: (1) Effective horizontal (effx) and vertical (effy) sizes of the fundamental, “f” ( $\phi_+$ ), and vortex, “v” ( $\phi_-$ ), components:

$$\{L_{\text{effx}}^{\text{f,v}}, L_{\text{effy}}^{\text{f,v}}\} = \left[ \frac{\iint \left\{ (x - X_{\text{mc}}^{\text{f,v}})^2, (y - Y_{\text{mc}}^{\text{f,v}})^2 \right\} |\phi_{+,-}(x, y)|^2 dx dy}{\iint |\phi_{+,-}(x, y)|^2 dx dy} \right]^{1/2}, \quad (14)$$

where  $\{X_{\text{mc}}^{\text{f,v}}, Y_{\text{mc}}^{\text{f,v}}\}$  are coordinates of the center of mass (c.o.m.) for the two components, which are defined as

$$\{X_{\text{mc}}^{\text{f,v}}, Y_{\text{mc}}^{\text{f,v}}\} = \frac{\iint \{x, y\} |\phi_{+,-}(x, y)|^2 dx dy}{\iint |\phi_{+,-}(x, y)|^2 dx dy}. \quad (15)$$

(2) The anisotropy of each component:

$$\eta_{+,-} = \frac{|L_{\text{effx}}^{(\text{f,v})} - L_{\text{effy}}^{(\text{f,v})}|}{L_{\text{effx}}^{(\text{f,v})} + L_{\text{effy}}^{(\text{f,v})}}. \quad (16)$$

(3) Norm shares of the fundamental and vortex components:

$$F_{+,-} = (N_{+,-}/N) \times 100\%. \quad (17)$$



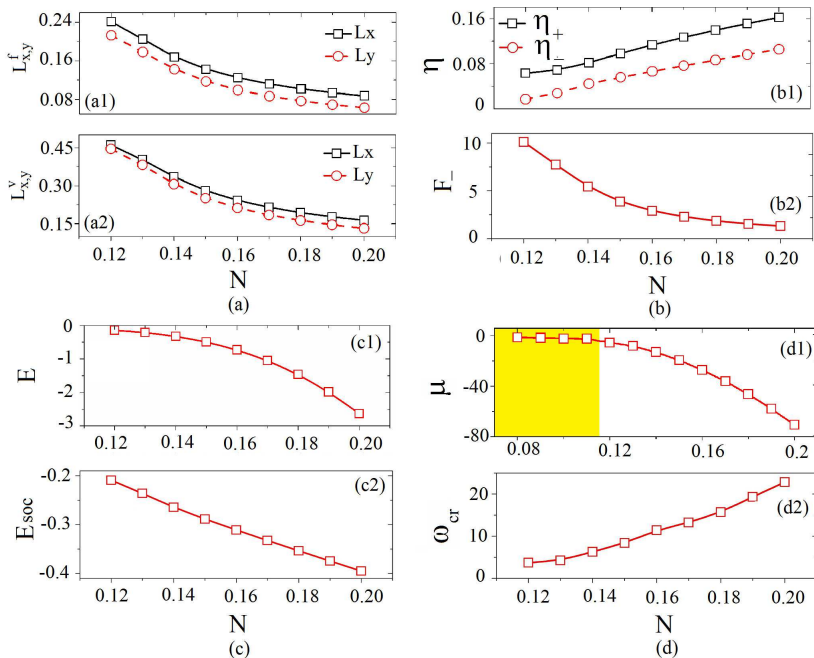


FIG. 2: (Color online) (a1,a2) Horizontal and vertical sizes [defined per Eq. (14)] versus  $N$  for the two SVS components. (b1) Anisotropies of both components,  $\eta_{\pm}$ , versus  $N$  [defined as per Eq. (16)]. (b2) The norm share of the vortical component of the SVS,  $F_-$ , versus  $N$  [defined as per Eq. (17)]. (c1,c2) The total energy of the SVS, and the energy of the spin-orbit coupling,  $E_{\text{SOC}}$ , versus  $N$ . (d1) The chemical potential of the SVS,  $\mu$ , versus  $N$ . In the yellow area, stationary SVSs are subject to the oscillatory instability, transforming into breathers which keep the same structure as the SVSs. (d2) The critical rotation speed,  $\omega_{\text{cr}}$ , versus  $N$ .

These characteristics, as well as the chemical potential [see Eq. (9)] and the total energy [see Eq. (11)] of the SVS are displayed versus the total norm in Fig. 2, at  $N \geq 0.12$ , where, as said above, the stationary SVSs are stable. Figure 2(a) demonstrates that, quite naturally, the SVS shrinks with the increase of  $N$ , its size in the  $x$ -direction being larger than along  $y$ , and the anisotropy degree,  $\eta_{+,-}$ , increases with  $N$ , see Fig. 2(b1). This finding can be easily explained by the fact that the increase of  $N$  leads to the domination of the nonlinear DDI, which tends to stretch 2D solitons along the  $x$  axis, as mentioned above. Further, Fig. 2(b2) demonstrates that the norm share of the vortical component,  $F_-$ , decreases with the growth of  $N$ , similar to what was found for stable semi-vortices in the system with the contact attraction [56]. In Fig. 2(c), the total energy of the SVS increases with  $N$ , whereas the SOC energy term decreases, hence the DDI energy plays the dominant role at large  $N$ . Finally, in Fig. 2(d1), the chemical potential decreases with  $N$ , hence the SVS family satisfies the Vakhitov-Kolokolov (VK) criterion,  $d\mu/dN < 0$ , which is a well-known necessary stability condition for any soliton family supported by attractive interactions [8, 9, 91]. The weak oscillatory instability of the SVS in the yellow (shaded) area of Fig. 2(d1) is not detected by the VK condition, which is sensitive only to instability accounted for by non-oscillatory perturbation modes.

### B. Mobility of the symmetric vortex solitons

Mobility of the SVS is a nontrivial issue, as the SOC terms break the Galilean invariance of the underlying equations (3). In this subsection, the mobilities of the soliton are studied by applying a kick to a stationary soliton solution,

$$\psi_{\pm}(\mathbf{r}, t = 0) = \phi_{\pm}(\mathbf{r}) \exp(i\mathbf{k} \cdot \mathbf{r}), \quad (18)$$

where  $\mathbf{k} = k_x \mathbf{i} + k_y \mathbf{j}$  is the vector of the kick. To study the resulting motion of the soliton, we define the trajectory of the moving soliton by time-dependent coordinates of the c.o.m of the fundamental component, as

$$\{X_{\text{mc}}^{\text{f}}(t), Y_{\text{mc}}^{\text{f}}(t)\} = \frac{\int \int \{x, y\} |\psi_{\pm}(x, y, t)|^2 dx dy}{\int \int |\psi_{\pm}(x, y, t)|^2 dx dy}. \quad (19)$$

Actually, the location of the c.o.m. is dominated by the fundamental component of the SVS, as the vortex components carries a much smaller norm, see Fig. 2(b2). The mobility of the kicked solitons were studied through the shape of the c.o.m. trajectories, as produced by real-time simulations of Eq. (3).

Three types of the motion have been identified, for different strengths of the kick applied along the  $x$ - and  $y$ -directions. Typical examples of them are displayed in Fig. 3(a,b,c). When the strength of the kick is smaller than a *depinning threshold*, the resulting trajectory is a circle, see a typical example in Fig. 3(a), which may be realized as produced by an effective Lorentz force acting upon the vortex component of the soliton. Up to the depinning threshold, the radius of the circular trajectory remains much smaller than the proper size of the soliton. The magnitude of the threshold is  $|\mathbf{k}| \approx 0.07$ , which is nearly constant in the range of  $0.12 < N < 0.2$ .

At  $|\mathbf{k}| > 0.07$ , the depinning of the soliton occurs, transforming the trajectory into a spiral, see a typical example in Fig. 3(b). In this case, the direction of the systematic drift of the soliton is opposite to the kick, hence this type of the dynamics may be considered as a superposition of progressive motion with a negative effective mass and circular motion. At  $|\mathbf{k}|$  exceeding a higher threshold value, the spiral trajectory is replaced by a complex one, as shown in Fig. 3(c). The magnitude of the upper threshold is  $|\mathbf{k}| = 0.46$ , which is also nearly constant for  $0.12 < N < 0.2$ .

At  $|\mathbf{k}|$  keeps growing, the increase of the absolute value of the drift velocity gives rise to an additional threshold value of the kick, at which the superposition of the drift with the circular motion changes the shape of spiral trajectory into a “lacy” one, as shown in Fig. 3(c). The magnitude of this threshold is  $|\mathbf{k}| = 0.46$ , which is also nearly constant for  $0.12 < N < 0.2$ . In Fig. 3(d), the mean velocity of the spiral motion of the solitons with  $N = 0.15$  and  $0.2$  are shown vs. the size of the kick, the dependences being very close for both values of  $N$ .

In Fig. 3(a,b), shifts of the soliton along the  $x$  and  $y$  directions, observed at  $t = 40$ , are nearly equal, implying that its mobility is nearly isotropic. However, in Fig. 3(c) it is seen that, for the kick with  $|k| = 0.5$ , which is larger than  $0.46$ , the  $x$  and  $y$  shifts,  $\Delta x \approx 4.8$  and  $\Delta y \approx 2.8$ , are different, which means that the mobility is anisotropic for the strong kick.

Although it may seem that the motion of the solitons observed in Fig. 3(b,c) violate the momentum conservation, the total vectorial (2D) momentum is actually conserved, in all the cases. To verify the momentum conservation, we define its normalized value as

$$\mathbf{M}(\mathbf{t}) = \frac{i \iint (\psi_+(t) \nabla \psi_+^*(t) + \psi_-(t) \nabla \psi_-^*(t)) dx dy}{\iint (|\psi_+(t)|^2 + |\psi_-(t)|^2) dx dy}. \quad (20)$$

The numerical results demonstrate that the so computed momentum remains constant, keeping the initial value which is equal to the kick applied to the soliton,  $M = k$ . An explanation to the complex motion of the soliton in Fig. 3(b,c) is the presence of small-amplitude radiation field, which plays the role of recoil which helps to conserve the total momentum.

## IV. ASYMMETRIC VORTEX SOLITONS (AVSS)

### A. Quiescent solitons

The model with the DDI interactions offers a completely novel feature, which was not found for semi-vortices in the 2D SOC system with the contact attractive interactions [56]: a possibility to produce stable AVSSs, with the asymmetry represented by spatial separation of the fundamental and vortical components. To produce such solutions in the quiescent form, we solved Eq. (3) by means of the imaginary-time-evolution method, with input

$$\phi_+^{(0)} = A_1 \exp(-\alpha_1 r^2), \quad \phi_-^{(0)} = A_2 |\mathbf{r} - \mathbf{R}_{\text{ps}}| \exp(i\theta_{\mathbf{r}_{\text{ps}}} - \alpha_2 r^2), \quad (21)$$

cf. Eq. (13), where  $\mathbf{R}_{\text{ps}} = X_{\text{ps}}^{\text{in}} \hat{i} + Y_{\text{ps}}^{\text{in}} \hat{j}$  is the initial offset of the vortex components with respect to the fundamental one, and  $\theta_{\mathbf{r}_{\text{ps}}}$  is the angular coordinate for the vortex’ pivot placed at  $\mathbf{r} = \mathbf{R}_{\text{ps}}$  (“ps” means “pivot shift”). Typical examples of the so generated stable AVSSs for  $N = 0.15$  are displayed in Fig. 4(a). In this figure, when we chose  $(X_{\text{ps}}^{\text{in}}, Y_{\text{ps}}^{\text{in}}) = (0.01, 0)$  and  $(0, 0.01)$ , the eventual (output) position of the pivot of the vortical component is at  $(X_{\text{ps}}^{\text{out}}, Y_{\text{ps}}^{\text{out}}) = (0.04, 0)$  and  $(0, 0.065)$ , respectively. To produce the relationship between  $(X_{\text{ps}}^{\text{out}}, Y_{\text{ps}}^{\text{out}})$  and  $(X_{\text{ps}}^{\text{in}}, Y_{\text{ps}}^{\text{in}})$ , we plot  $X_{\text{ps}}^{\text{out}}$  versus  $X_{\text{ps}}^{\text{in}}$  in Fig. 4(b2) (the respective dependence for the offset along  $y$  is not shown here, as it is almost identical to that produced by the offset in the  $x$  direction). The figure shows that  $X_{\text{ps}}^{\text{out}}$  saturates to  $0.47$  with the increase of  $X_{\text{ps}}^{\text{in}}$ , in the case of  $N = 0.15$ . Further, the maximum output offset along  $x$ -axis,  $X_{\text{ps}}^{\text{max}}$ , i.e., the saturation value of the offset, is displayed as a function of  $N$  in Fig. 4(b3). It decreases with the increase of  $N$  because the semi-vortex itself shrinks with the growth of  $N$ . At  $N < 0.12$ , the AVSSs takes the form of a robust breather, similar to what is shown above for the SVS.

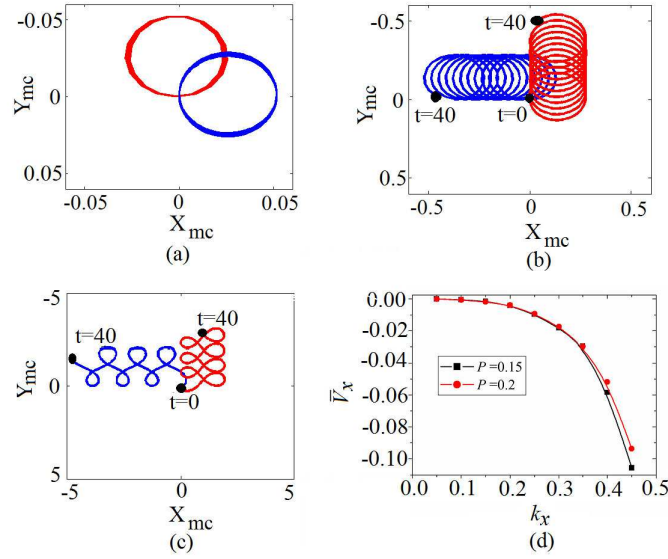


FIG. 3: (Color online) (a,b,c) Trajectories of the fundamental c.o.m. of the soliton kicked by  $\mathbf{k} \equiv (k_x, k_y) = (0.05, 0)$  (blue cycle) &  $(0, 0.05)$  (red cycle) [panel (a)],  $(0.25, 0)$  (blue spiral) &  $(0, 0.25)$  (red spiral) [panel (b)] and  $(0.5, 0)$  (blue lacy curve) &  $(0, 0.5)$  (red lacy curve) [panel (c)], respectively. In all the cases, the soliton's norm is  $N = 0.15$ . In these panels, the evolution time is  $t = 40$ . Panel (d) displays the mean velocity of the spiral motion of the soliton versus  $k_x$  for  $N = 0.15$  and  $N = 0.2$ , respectively.  $\bar{V}_x < 0$  means that the soliton moves against the direction of the applied kick.

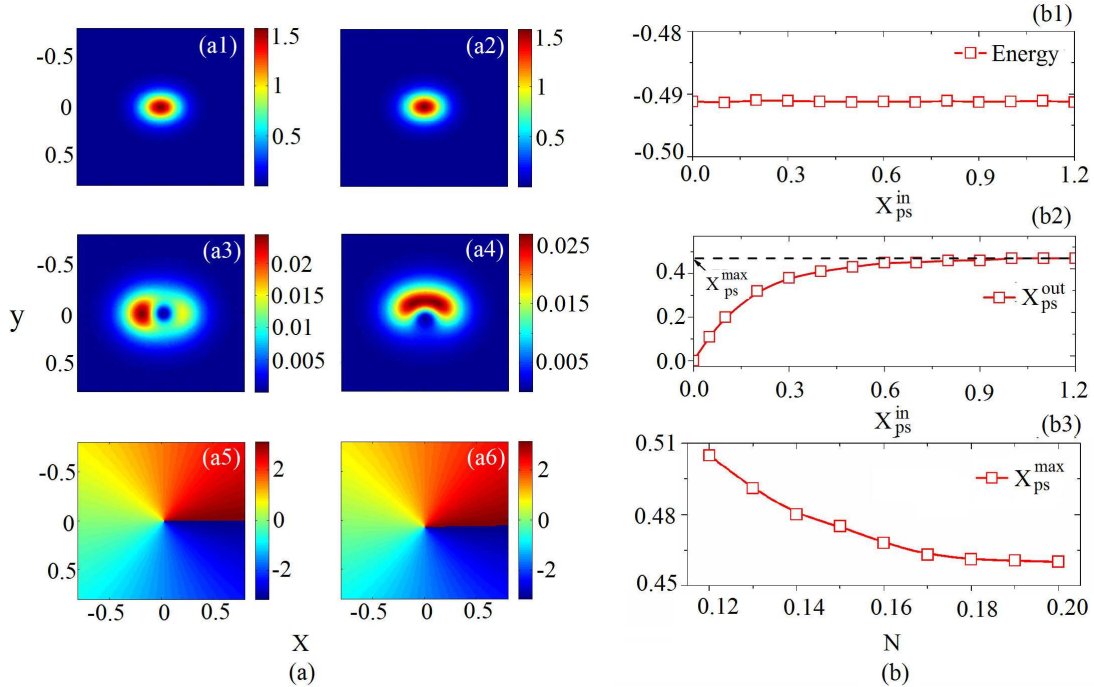


FIG. 4: (Color online) (a1-a4) Typical examples of the density profile in the fundamental (a1,a2) and vortical (a3,a4) component,  $\phi_+$  and  $\phi_-$ , of a stable AVS, for the initial offset of the vortex' pivot with respect to the fundamental component  $(X_{ps}^{in}, Y_{ps}^{in}) = (0.01, 0)$  and  $(0, 0.01)$ , respectively. The origin of the coordinate system is placed at the final position of the pivot. The total norm of the asymmetric semi-vortex soliton is  $N = 0.15$ . (a5,a6) The phase structure of the vortical components ( $\psi_-$ ) from panels (a3) and (a4), respectively. The output values of the pivot's offset of these two AVSs are  $(X_{ps}^{out}, Y_{ps}^{out}) = (0.04, 0)$  and  $(0, 0.065)$ , respectively. (b1) The energy of the AVS versus  $X_{ps}^{in}$ , showing the degeneracy of the family. (b2)  $X_{ps}^{out}$  versus  $X_{ps}^{in}$ , the saturation taking place at the largest output offset  $X_{ps}^{max} = 0.47$ , for the AVS with  $N = 0.15$ . (b3) The largest output offset of the vortex' pivot along the  $x$ -axis,  $X_{ps}^{out}$ , versus  $N$ .



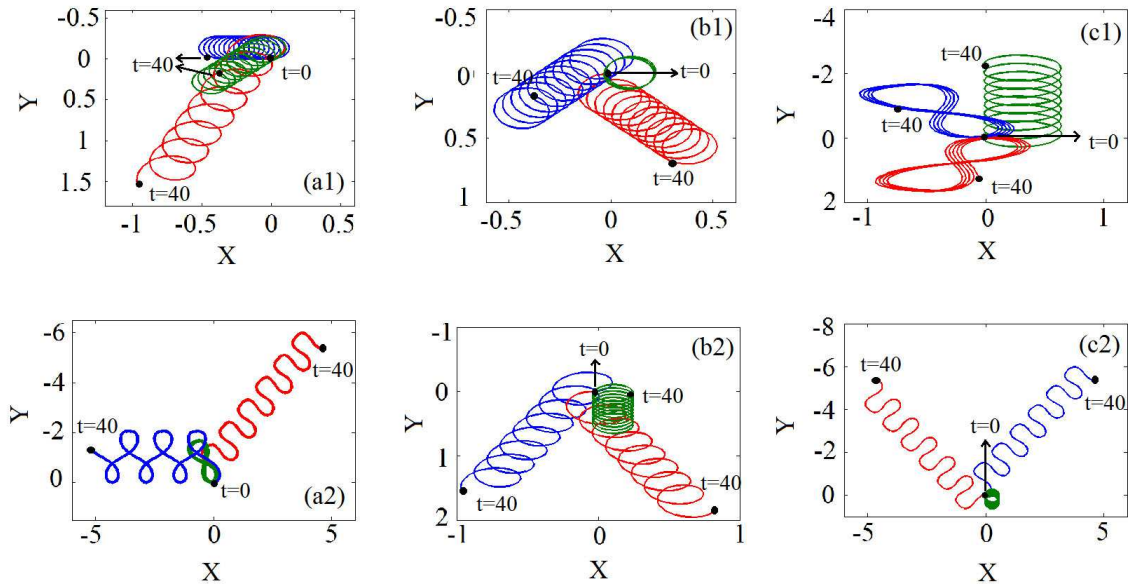


FIG. 5: (Color online) (a1,a2) Trajectories of AVSs, with  $(X_{\text{ps}}^{\text{out}}, Y_{\text{ps}}^{\text{out}}) = (0, 0)$  (blue curves),  $(0.12, 0)$  (green curves) and  $(0.26, 0)$  (red curves), produced by the application of the kick  $\mathbf{k} \equiv (k_x, k_y) = (+0.25, 0)$  (a1) and  $(+0.5, 0)$  (a2), respectively. (b1,b2) Trajectories of the AVSs with  $(X_{\text{ps}}^{\text{out}}, Y_{\text{ps}}^{\text{out}}) = (0.12, 0)$  (b1) and  $(0.26, 0)$  (b2), kicked by  $\mathbf{k} \equiv (k_x, k_y) = (+0.25, 0)$  (blue curves),  $(-0.25, 0)$  (red curves) and  $(0, +0.25)$  (green curves). (c1,c2) Trajectories of the AVSs with  $(X_{\text{ps}}^{\text{out}}, Y_{\text{ps}}^{\text{out}}) = (0.12, 0)$  (c1) and  $(0.26, 0)$  (c2) kicked by  $\mathbf{k} \equiv (k_x, k_y) = (+0.5, 0)$  (blue curves),  $(-0.5, 0)$  (red curves) and  $(0, +0.5)$  (green curves).

To the best of our knowledge, such a species of AVS was not previously reported in other 2D nonlinear models. Thus, we conclude that, for given total norm  $N$ , instead of the single stable SVS (alias semi-vortex), which was recently found in the system combining the SOC and contact attractive interactions [56], there exists a *continuous family* of AVSs, parameterized by the offsets of the vortex' pivot,  $X_{\text{ps}}^{\text{out}}$  and  $Y_{\text{ps}}^{\text{out}}$ , that take values from 0 to  $X_{\text{ps}}^{\text{max}}$ . The calculation of the total energy (11) [see Fig. 4(b1)] demonstrates that its values are almost constant for all the AVSs with the same norm, which seems as continuous degeneracy of the ground state (very small fluctuations in this figure, at a level of  $< 10^{-5}$ , are produced by numerical-truncation errors, which may be safely disregarded safely). Such continuous degeneracy suggests a possibility of the existence of a hidden symmetry, which, however, we were not able to find. A rough explanation to the degeneracy is that the nonlocal character of the DDI may smoothen the difference in the energy for the modes with various spatial structures. These results suggest more possibilities for the creation of stable 2D solitons in the experiment.

## B. Mobility of the asymmetric vortex solitons

Similar to what was done above for SVSs, the mobility of the AVSs was numerically studied by applying kick to it, as per Eq. (18). The numerical simulations demonstrate that the computed momentums, which are defined as per Eq. (20), for the moving AVSs remain constant too. Typical examples of the respective mobility are displayed in Fig. 5 by means of trajectories of the c.o.m of the AVS's fundamental component, which are defined as per Eq. (19).

Figure 5 demonstrates that the dynamics of the kicked AVSs is more complex than that of their SVS counterparts. First, Fig. 5(a1) shows that the application of the horizontal kick to the soliton with  $X_{\text{ps}}^{\text{out}} \neq 0$  induces not only horizontal motion, but also motion in the vertical direction, whose velocity increases with the increase of  $X_{\text{ps}}^{\text{out}}$ . Next, the shape of the trajectories initiated by a strong kick becomes completely different. For example, in panel Fig. 5(a2), the trajectory of the SVSs with  $X_{\text{ps}}^{\text{out}} = 0$  has a “lacy” form (cf. blue color curve), directed in the negative  $x$ -direction, while the AVS with  $X_{\text{ps}}^{\text{out}} = 0.12$  moves around the origin along a nearly closed figure-of-eight trajectory (cf. green color curve), and the the trajectory of the AVS with  $X_{\text{ps}}^{\text{out}} = 0.26$  changes into a “zipper” directed along the diagonal formed by positive  $x$  and negative  $y$  directions (cf. red color curve). Further, the motion of the kicked AVSs shows stronger anisotropy than the SVSs when the kick is applied along the horizontal and vertical directions. Typical examples of this are displayed in Figs. 5(b1, b2, c1, c2) [panels (b1,c1) correspond to  $X_{\text{ps}}^{\text{out}} = 0.12$  and panels (b2,

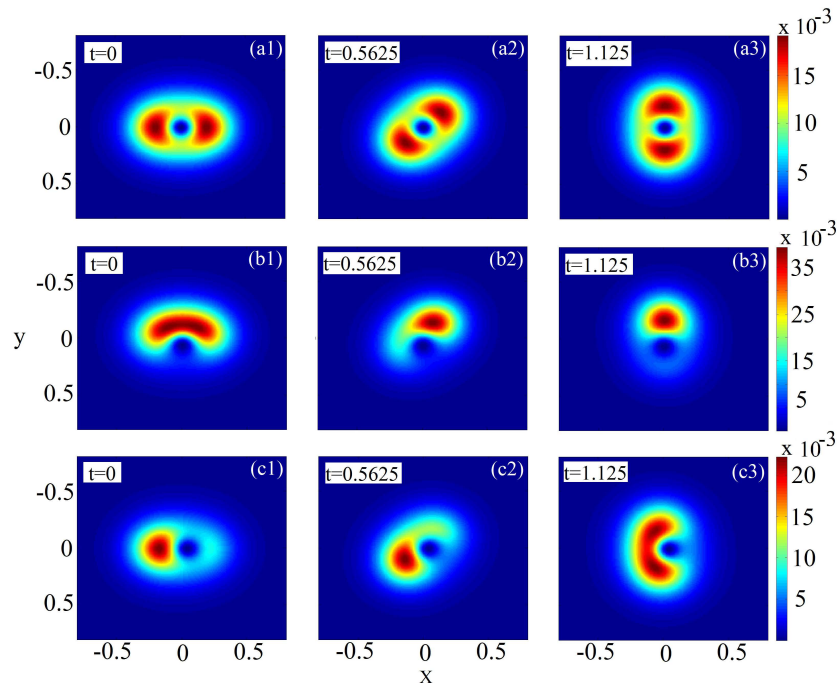


FIG. 6: (Color online) The stable rotation of the vortical component of the semi-vortex solitons driven by the rotating magnetic field. (a1-a3) The symmetric semi-vortex. (b,c) Asymmetric semi-vortices, with  $(X_{\text{ps}}^{\text{out}}, Y_{\text{ps}}^{\text{out}}) = (0.04, 0)$  and  $(X_{\text{ps}}^{\text{out}}, Y_{\text{ps}}^{\text{out}}) = (0, 0.065)$ , respectively. The rotation speed is  $\omega = 0.45\pi$ , and the total norm of each semi-vortex soliton is  $N = 0.15$ . The respective evolution of the fundamental component is not shown, as it is less conspicuous.

c2) to  $X_{\text{ps}}^{\text{out}} = 0.26$ ]. The green trajectories in these panels pertain to the kick applied along the positive  $y$ -direction, while the blue and red trajectories pertain to the kicks along the positive and negative  $x$ -directions, respectively. In the latter case (the horizontal kicks), the blue and red trajectories feature similar shapes. However, the vertical kick, unlike the horizontal ones, does not induce diagonal motion; instead, the trajectories form vertical spirals.

## V. ROTATION OF THE SEMI-VORTEX SOLITONS

Systems in which 2D solitons are supported by the DDI make it possible to consider dynamical generalizations of such solitons, assuming that the external magnetic field, which polarizes the magnetic moments, rotates at a finite angular velocity,  $\omega$ , hence the atomic moments tend to follow it [77, 78]. In the present system, the rotation may be naturally introduced by replacing  $\Theta \rightarrow \Theta + \omega t$  in Eq. (4). Figure 6 shows that the magnetic polarizations of both SVs and AVs can stably follow the rotation of the driving field.

For a fixed value of the total norm, there is a critical angular speed,  $\omega_{\text{cr}}$ , beyond which the soliton is not able to follow rotation of the polarizing field, and gets destroyed (a similar effect was reported in Ref. [77, 78]). Figure 2(d2) displays  $\omega_{\text{cr}}$  as a function of  $N$ , suggesting that the semi-vortex solitons are more robust, following the spinning external field, when the nonlocal nonlinearity is stronger. Indeed, being dragged by the rotating field, the 2D anisotropic soliton must overcome the resistance of the SOC-induced pinning, which is easier to do when the linear SOC terms are relatively weak in comparison with the DDI.

## VI. CONCLUSION

The objective of this work is to construct stable 2D anisotropic solitary vortices in the model of the spinor BEC composed of atoms carrying permanent magnetic moments, with the SOC (spin-orbit coupling) applied to the two components of the spinor wave function. The nonlinearity is represented by the DDI (dipole-dipole interaction) between the magnetic moments polarized in the system's plane, while the contact nonlinearity is assumed to be negligible. Following the recent prediction of stable 2D solitons in the form of semi-vortices in the SOC system

combined with the contact attractive interactions [56], we have demonstrated that the DDI supports stable semi-vortex solitons in the present setting. The most essential novelty in comparison with the case of the local isotropic interactions is that, for a given total norm of the soliton, the system with the DDI gives rise to continuous families of stable AVSs (asymmetric (semi-)vortex solitons) parameterized by the offset of the vortex' pivot from the soliton's fundamental component, instead of the single SVS (symmetric (semi-)vortex soliton) found in the system with the contact attraction. To the best of our knowledge, such composite solitons, with linearly coupled but spatially separated fundamental and vortex components, were not previously discovered in any other 2D nonlinear system. In addition, the mobility of the solitons was studied by applying the kick to them. The solitons have a negative effective mass, moving in the direction opposite to the kick, provided that its strength exceeds the critical (depinning) value. The critical angular velocity was found too, up to which the 2D semi-vortices may follow the rotation of the external magnetic field that determines the polarization of the atomic magnetic moments.

The present analysis can be extended in various directions. First, Ref. [56] suggests to look for another class of composite solitons, namely, mixed modes, which include fundamental and vortical terms in both components, and feature small separation between maxima of the two components. Further, it may be interesting to consider effects of the competition of the DDI and contact interactions, that may be added to the system. Further, the existence of stably moving solitons suggest a possibility to simulate collisions between them [56]. Finally, a challenging option is to seek for stable solitons in the 3D setting with SOC, as suggested by the recent discovery of such 3D objects in the model with the contact attractive nonlinearity [92].

### Acknowledgments

This work was supported, in a part, by the National Natural Science Foundation of China through Grants 11575063 and 11547212.

- 
- [1] B. A. Malomed, D. Mihalache, F. Wise, and L. Torner, Spatiotemporal optical solitons, *J. Optics B: Quant. Semicl. Opt.* **7**, R53 (2005).
  - [2] A. S. Desyatnikov, L. Torner, and Y. S. Kivshar, Optical Vortices and Vortex Solitons, *Prog. Opt.* **47**, 1 (2005).
  - [3] Y. S. Kivshar and G. P. Agrawal, *Optical Solitons: From Fibers to Photonic Crystals* (Academic Press San Diego)
  - [4] S. E. Pollack, D. Dries, M. Junker, Y. P. Chen, T. A. Corcovilos, and R. G. Hulet, Extreme tunability of interactions in a  $^7\text{Li}$  Bose-Einstein condensate, *Phys. Rev. Lett.* **102**, 090402 (2009).
  - [5] D. M. Bauer, M. Lettner, C. Vo, G. Rempe and S Dür, Control of a magnetic Feshbach resonance with laser light, *Nature Phys.* **5**, 339 (2009).
  - [6] M. Yan, B. J. DeSalvo, B. Ramachandran, H. Pu, and T. C. Killian, Controlling condensate collapse and expansion with an optical Feshbach resonance, *Phys. Rev. Lett.* **110**, 123201 (2013).
  - [7] G. Fibich and G. Papanicolaou, Self-focusing in the perturbed and unperturbed nonlinear Schrödinger equation in critical dimension, *SIAM J. Appl. Math.* **60**, 183 (1999).
  - [8] L. Bergé, Wave collapse in physics: principles and applications to light and plasma waves, *Phys. Rep.* **303**, 259 (1998).
  - [9] E. A. Kuznetsov and F. Dias, Bifurcations of solitons and their stability, *Phys. Rep.* **507**, 43 (2011).
  - [10] W. E. Torruellas, Z. Wang, D. J. Hagan, E. W. VanStryland, G. I. Stegeman, L. Torner and C. R. Menyuk, Observation of Two-Dimensional Spatial Solitary Waves in a Quadratic Medium, *Phys. Rev. Lett.* **74**, 5036 (1995).
  - [11] B. A. Malomed, P. Drummond, H. He, A. Berntson, D. Anderson, and M. Lisak, Spatio-temporal solitons in optical media with a quadratic nonlinearity, *Phys. Rev. E* **56**, 4725 (1997).
  - [12] X. Liu, K. Beckwitt and F. Wise, Two-dimensional optical spatiotemporal solitons in quadratic media, *Phys. Rev. E* **62**, 1328 (2000).
  - [13] W. J. Firth and D. V. Skryabin, Optical solitons carrying orbital angular momentum, *Phys. Rev. Lett.* **79**, 2450 (1997).
  - [14] L. Torner, D. Petrov, Azimuthal instabilities and self-breaking of beams into sets of solitons in bulk second-harmonic generation, *Electron. Lett.* **33**, 608 (1997).
  - [15] M. Quiroga-Teixeiro and H. Michinel, Stable azimuthal stationary state in quintic nonlinear optical media, *J. Opt. Soc. Am. B* **14**, 2004 (1997).
  - [16] K. Dimitrevski, E. Reimhult, E. Svensson, A. Öhgren, D. Anderson, A. Berntson, M. Lisak, M. L. Quiroga-Teixeiro, Analysis of stable self-trapping of laser beams in cubic-quintic nonlinear media, *Phys. Lett. A* **248**, 369 (1998).
  - [17] R. L. Pego and H. A. Warchall, Spectrally stable encapsulated vortices for nonlinear Schrödinger equations, *J. Nonlin. Sci.* **12**, 347 (2002).
  - [18] D. Mihalache, D. Mazilu, L-C. Crasovan, I. Towers, A. V. Buryak, B. A. Malomed, A. Torner, J. P. Torres, and F. Lederer, Stable spinning optical solitons in three dimensions, *Phys. Rev. Lett.* **88**, 073902 (2002).

- [19] D. Mihalache, D. Mazilu, L-C. Crasovan, I. Towers, B. A. Malomed, A. V. Buryak, L. Torner, and F. Lederer, Stable three-dimensional spinning optical solitons supported by competing quadratic and cubic nonlinearities, *Phys. Rev. E* **66**, 016613 (2002).
- [20] E. L. Falcão-Filho, C. B. de Araújo, G. Boudebs, H. Leblond, V. Skarka, Robust two-dimensional spatial solitons in liquid carbon disulfide, *Phys. Rev. Lett.* **110**, 013901 (2013).
- [21] N. K. Efremidis, S. Sears, D. N. Christodoulides, J. W. Fleischer, and M. Segev, Discrete solitons in photorefractive optically induced photonic lattices, *Phys. Rev. E* **66**, 046602 (2002).
- [22] A. Szameit, J. Burghoff, T. Pertsch, S. Nolte, A. Tünnermann, and F. Lederer, Two-dimensional soliton in cubic fs laser written waveguide arrays in fused silica, *Opt. Exp.* **14**, 6055 (2006).
- [23] O. Morsch and N. Oberthaler, Dynamics of Bose-Einstein condensates in optical lattices, *Rev. Mod. Phys.* **78**, 179 (2006).
- [24] J. W. Fleischer, M. Segev, N. K. Efremidis, and D. N. Christodoulides, Observation of two-dimensional discrete solitons in optically induced nonlinear photonic lattices, *Nature* **422**, 147 (2003).
- [25] D. Neshev, T. J. Alexander, E. A. Ostrovskaya, Y. S. Kivshar, H. Martin, I. Makasyuk, and Z. Chen, Observation of discrete vortex solitons in optically induced photonic lattices, *Phys. Rev. Lett.* **92**, 123903 (2004).
- [26] J. W. Fleischer, G. Bartal, O. Cohen, O. Manela, M. Segev, J. Hudock, and D. N. Christodoulides, Observation of vortex-ring “discrete” solitons in 2D photonic lattices, *Phys. Rev. Lett.* **92**, 23904 (2004).
- [27] B. Terhalle, T. Richter, K. J. H. Law, D. Görjes, P. Rose, T. J. Alexander, P. G. Kevrekidis, A. S. Desyatnikov, W. Królikowski, F. Kaiser, C. Denz, and Y. S. Kivshar, Observation of double-charge discrete vortex solitons in hexagonal photonic lattices, *Phys. Rev. A* **79**, 043821 (2009).
- [28] S. Minardi, F. Eilenberger, Y. V. Kartashov, A. Szameit, Röpke U, J. Kobelke, K. Schuster, H. Bartelt, S. Nolte, L. Torner, F. Lederer, A. Tünnermann, and T. Pertsch, Three-dimensional light bullets in arrays of waveguides, *Phys. Rev. Lett.* **105**, 263901 (2010).
- [29] E. A. Cerda-Méndez, D. Sarkar, D. N. Krizhanovskii, S. S. Gavrilov, K. Biermann, M.S. Skolnick, and P. V. Santos, Exciton-polariton gap solitons in two-dimensional lattices, *Phys. Rev. Lett.* **111**, 146401 (2013).
- [30] B. A. Malomed, *Soliton Management in Periodic Systems*, (Springer: New York) (2006).
- [31] I. Towers and B. A. Malomed, Stable (2+1)-dimensional solitons in a layered medium with sign-alternating Kerr nonlinearity, *J. Opt. Soc. Am. B* **19**, 537 (2002).
- [32] F. Kh. Abdullaev, J. G. Caputo, R. A. Kraenkel, and B. A. Malomed, Controlling collapse in Bose-Einstein condensation by temporal modulation of the scattering length, *Phys. Rev. A* **67**, 013605 (2003).
- [33] H. Saito and M. Ueda, Dynamically stabilized bright solitons in a two-dimensional Bose-Einstein condensate, *Phys. Rev. Lett.* **90**, 040403 (2005).
- [34] G. D. Montesinos, V. M. Pérez-García, H. Michinel, and J. R. Salgueiro, Stabilized vortices in layered Kerr media, *Phys. Rev. E* **71**, 036624 (2005).
- [35] O. V. Borovkova, Y. V. Kartashov, B. A. Malomed, and L. Torner, Algebraic bright and vortex solitons in defocusing media, *Opt. Lett.* **36**, 3088 (2011).
- [36] O. V. Borovkova, Y. V. Kartashov, L. Torner, and B. A. Malomed, Bright solitons from defocusing nonlinearities, *Phys. Rev. E* **84**, 035602 (2011).
- [37] R. Driben, Y. V. Kartashov, B. A. Malomed, T. Meier, and L. Torner, Soliton gyroscopes in media with spatially growing repulsive nonlinearity, *Phys. Rev. Lett.* **112**, 020404 (2014).
- [38] Q. Tian, L. Wu, Y. Zhang, and J-F. Zhang, Vortex solitons in defocusing media with spatially inhomogeneous nonlinearity, *Phys. Rev. E* **85**, 056603 (2012).
- [39] Y. Wu, Q. Xie, H. Zhong, L. Wen, and W. Hai, Algebraic bright and vortex solitons in self-defocusing media with spatially inhomogeneous nonlinearity, *Phys. Rev. Lett.* **87**, 055801 (2013).
- [40] Y. V. Kartashov, B. A. Malomed, Y. Shnir, and L. Torner, Twisted toroidal vortex-solitons in inhomogeneous media with repulsive nonlinearity, *Phys. Rev. Lett.* **113**, 264101 (2014).
- [41] Y. J. Lin, K. Jiménez-García, and I. B. Spielman, Spin-orbit-coupled Bose-Einstein condensates, *Nature* **471**, 83 (2011).
- [42] Y. Zhang, L. Mao, and C. Zhang, Mean-field dynamics of spin-orbit coupled Bose-Einstein condensates, *Phys. Rev. Lett.* **108**, 035302 (2012).
- [43] H. Zhai, Spin-orbit coupled quantum gases, *Int. J. Mod. Phys. B* **26**, 1230001 (2012).
- [44] Sh. Mardonov, M. Modugno, and E. Ya. Sherman, Dynamics of spin-orbit coupled Bose-Einstein condensates in a random potential, *Phys. Rev. Lett.* **115**, 180402 (2015).
- [45] X-Q. Xu and J. H. Han, Spin-orbit coupled Bose-Einstein condensate under rotation, *Phys. Rev. Lett.* **107**, 200401 (2011).
- [46] S. Sinha, R. Nath, and L. Santos, Trapped two-dimensional condensates with synthetic spin-orbit coupling, *Phys. Rev. Lett.* **107**, 270401 (2011).
- [47] J. Radić, T. A. Sedrakyan, I. B. Spielman, and V. Galitski, Vortices in spin-orbit-coupled Bose-Einstein condensates, *Phys. Rev. A* **84**, 063604 (2011).
- [48] X. F. Zhou, J. Zhou, and C. J. Wu, Vortex structures of rotating spin-orbit-coupled Bose-Einstein condensates, *Phys. Rev. Lett.* **84**, 063624 (2011).
- [49] H. Sakaguchi and B. Li, Vortex lattice solutions to the Gross-Pitaevskii equation with spin-orbit coupling in optical lattices, *Phys. Rev. Lett.* **87**, 015602 (2013).
- [50] Y. V. Kartashov, V. V. Konotop, and F. Kh. Abdullaev, Gap solitons in a spin-orbit-coupled Bose-Einstein condensate, *Phys. Rev. Lett.* **111**, 060402 (2013).
- [51] V. E. Lobanov, Y. V. Kartashov, and V. V. Konotop, Fundamental, multipole and half-vortex gap solitons in spin-orbit coupled Bose-Einstein condensates. *Phys. Rev. Lett.* **112**, 180403 (2014).



- [52] P. Beličev, G. Gligorić, J. Petrović, A. Maluckov, L. Hadzievski, and B. A. Malomed, Composite localized modes in discretized spin-orbit-coupled Bose-Einstein condensates, *J. Phys. B* **48**, 065301 (2015).
- [53] Y. Xu, Y. Zhang, and B. Wu, Bright solitons in spin-orbit-coupled Bose-Einstein condensates, *Phys. Rev. A* **87**, 013614 (2013).
- [54] V. Achilleos, D. J. Frantzeskakis, P. G. Kevrekidis, and D. E. Pelinovsky, Matter-wave bright solitons in spin-orbit coupled Bose-Einstein condensates, *Phys. Rev. Lett.* **110**, 264101 (2013).
- [55] L. Salasnich and B. A. Malomed, Localized modes in dense repulsive and attractive Bose-Einstein condensates with spin-orbit and Rabi couplings, *Phys. Rev. A* **87**, 063625 (2013).
- [56] H. Sakaguchi, B. Li, and B. A. Malomed, Creation of two-dimensional composite solitons in spin-orbit-coupled self-attractive Bose-Einstein condensates in free space. *Phys. Rev. E* **89**, 032920 (2014).
- [57] H. Sakaguchi and B. A. Malomed, Discrete and continuum composite solitons in Bose-Einstein condensates with the Rashba spin-orbit coupling in one and two dimensions, *Phys. Rev. E* **90**, 062922 (2014).
- [58] L. Salasnich, W. B. Cardoso, and B. A. Malomed, Localized modes in quasi-two-dimensional Bose-Einstein condensates with spin-orbit and Rabi couplings, *Phys. Rev. A* **90**, 033629 (2014).
- [59] Y. M. Kartashov, B. A. Malomed, V. V. Konotop, V. E. Lobanov, and L. Torner, Stabilization of solitons in bulk Kerr media by dispersive coupling, *Opt. Lett.* **40**, 1045 (2015).
- [60] M. Peccianti, K. A. Brzdakiewicz, and G. Assanto, Nonlocal spatial soliton interactions in nematic liquid crystals, *Opt. Lett.* **27**, 1460 (2002).
- [61] C. Conti, M. Peccianti, and G. Assanto, Route to nonlocality and observation of accessible solitons, *Phys. Rev. Lett.* **91**, 073901 (2003).
- [62] C. Conti, M. Peccianti, and G. Assanto, Observation of optical spatial solitons in a highly nonlocal medium, *Phys. Rev. Lett.* **92**, 113902 (2004).
- [63] S. Skupin, O. Bang, D. Edmundson, and W. Królikowski, Stability of two-dimensional spatial solitons in nonlocal nonlinear media, *Phys. Rev. E* **73**, 066603 (2006).
- [64] A. Minovich, D. M. Neshev, A. Dreischuh, W. Królikowski, and Y. S. Kivshar, Experimental reconstruction of nonlocal response of thermal nonlinear optical media, *Opt. Lett.* **32**, 1599 (2007).
- [65] P. D. Rasmussen, F. H. Bennet, D. N. Neshev, A. A. Sukhorukov, C. R. Rosberg, W. Królikowski, O. Bang, and Y. S. Kivshar, Observation of two-dimensional nonlocal gap solitons, *Opt. Lett.* **34**, 295 (2009).
- [66] R. Heidemann, U. Raitzsch, V. Bendkowsky, B. Butscher, W. R. Lö, and T. Pfau, Rydberg excitation of Bose-Einstein condensates, *Phys. Rev. Lett.* **100**, 033601 (2008).
- [67] A. Griesmaier, J. Werner, S. Hensler, J. Stuhler, and T. Pfau, Bose-Einstein condensation of Chromium, *Phys. Rev. Lett.* **94**, 160401 (2005).
- [68] M. Lu, N. Q. Burdick, S. H. Youn, and B. L. Lev, Strongly dipolar Bose-Einstein condensate of dysprosium, *Phys. Rev. Lett.* **107**, 190401 (2011).
- [69] K. Aikawa, A. Frisch, M. Mark, S. Baier, A. Rietzler, R. Grimm, and F. Ferlaino, Bose-Einstein condensation of Erbium, *Phys. Rev. Lett.* **108**, 210401 (2012).
- [70] T. Lahaye, C. Menotti, L. Santos, M. Lewenstein, and T. Pfau, The physics of dipolar bosonic quantum gases, *Rep. Prog. Phys.* **72**, 126401 (2009).
- [71] J. Cuevas, B. A. Malomed, P. G. Kevrekidis, and D. J. Frantzeskakis, Solitons in quasi-one-dimensional Bose-Einstein condensates with competing dipolar and local interactions, *Phys. Rev. A* **79**, 053608 (2009).
- [72] T. Bland, M. J. Edmonds, N. P. Proukakis, A. M. Martin, D. H. J. O'Dell, and N. G. Parker, Controllable nonlocal interactions between dark solitons in dipolar condensates, *Phys. Rev. A* **92**, 063601 (2015).
- [73] P. Pedri and L. Santos, Two-dimensional bright solitons in dipolar Bose-Einstein condensates, *Phys. Rev. Lett.* **95**, 200404 (2005).
- [74] R. Nath, P. Pedri, and L. Santos, Stability of dark Solitons in three-dimensional dipolar Bose-Einstein condensates, *Phys. Rev. Lett.* **101**, 210402 (2008).
- [75] I. Tikhonenkov, B. A. Malomed, and A. Vardi, Vortex solitons in dipolar Bose-Einstein condensates, *Phys. Rev. A* **78**, 043614 (2008).
- [76] Y. Li, J. Liu, W. Pang and B. A. Malomed, Matter-wave solitons supported by field-induced dipole-dipole repulsion with a spatially modulated strength, *Phys. Rev. A* **88**, 053630 (2013)
- [77] I. Tikhonenkov, B. A. Malomed, and A. Vardi, Anisotropic solitons in dipolar Bose-Einstein Condensates, *Phys. Rev. Lett.* **100**, 090406 (2008).
- [78] P. Köberle, D. Zajec, G. Wunner, and B. A. Malomed, Creating two-dimensional bright solitons in dipolar Bose-Einstein condensates, *Phys. Rev. A* **85**, 023630 (2012).
- [79] Y. Deng, J. Cheng, H. Jing, C. P. Sun, and S. Yi, Spin-orbit-coupled dipolar Bose-Einstein condensates, *Phys. Rev. Lett.* **108**, 125301 (2012).
- [80] R. M. Wilson, B. M. Anderson, and C. W. Clark, Meron ground state of Rashba spin-orbit-coupled dipolar bosons, *Phys. Rev. Lett.* **111**, 185303 (2013).
- [81] S-W. Song, L. Wen, C. F. Liu, S. G. Gou, and W-M. Liu, Ground states, solitons and spin textures in spin-1 Bose-Einstein condensates, *Front. Phys.* **8**, 302 (2013).
- [82] Y. Xu, Y. Zhang, and C. Zhang, Bright solitons in a 2D spin-orbit-coupled dipolar Bose-Einstein condensate, *Phys. Rev. A* **92**, 013633 (2005).
- [83] A. S. Desyatnikov, A. A. Sukhorukov, and Y. S. Kivshar, Azimuthons: Spatially modulated vortex solitons, *Phys. Rev. Lett.* **95**, 203904 (2005).



- [84] V. M. Lashkin, Stable three-dimensional spatially modulated vortex solitons in Bose-Einstein condensates, *Phys. Rev. A* **78**, 033603 (2008).
- [85] Y. Zhang, Y. Skupin, F. Maucher, A. Galestian Pour, K. Lu, and KróW. likowski, Azimuthons in weakly nonlinear waveguides of different symmetries, *Opt. Exp.* **18**, 27846 (2010).
- [86] X-j. Lai, C-Q. Dai, X-o Cai, and J-F. Zhang, Azimuthally modulated vortex solitons in bulk dielectric media with a Gaussian barrier *Opt. Commun.* **353**, 101 (2015).
- [87] Y. V. Izdebskaya, A. S. Desyatnikov, G. Assanto, and Y. S. Kivshar, Dipole azimuthons and vortex charge flipping in nematic liquid crystals, *Opt. Exp.* **19**, 21457 (2011).
- [88] J. Huang, X. Jiang, H. Chen, Z. Fan, W. Pang and Y. Li, Quadrupolar matter-wave soliton in two-dimensional free space, *Front. Phys.* **10**, 100507 (2015).
- [89] L. M. Chiofalo, S. Succi, and P. M. Tosi, Ground state of trapped interacting Bose-Einstein condensates by an explicit imaginary-time algorithm, *Phys. Rev. E* **62**, 7438 (2000).
- [90] J. Yang and T. I. Lakoba, Accelerated imaginary-time evolution methods for the computation of solitary waves, *Stud. Appl. Math.* **120**, 265 (2008).
- [91] N. G. Vakhitov and A. A. Kolokolov, Stationary solutions of the wave equation in a medium with nonlinearity saturation, *Radiophys. Quantum Electron.* **16**, 783 (1973).
- [92] Y.-C. Zhang, Z.-W. Zhou, B. A. Malomed, and H. Pu, Stable solitons in three dimensional free space without the ground state: Self-trapped Bose-Einstein condensates with spin-orbit coupling, *Phys. Rev. Lett.* **115**, 253902 (2015).